Ceilometers as planetary boundary layer height detectors and a corrective tool for ECMWF and COSMO NWP models

Leenes Uzan[1,2], Smadar Egert[1], Pavel Khain[2], Yoav Levi[2], Elyakom Vladislavsky[2], Pinhas Alpert[1]

[1] Porter School of the Environment and Earth Sciences, Raymond and Beverly Sackler Faculty of Exact Sciences, Tel-Aviv University, Tel Aviv, 6997801, Israel.
[2] The Israeli Meteorological Service, Beit Dagan, Israel.

Correspondence to: Leenes Uzan (Leenesu@gmail.com)

Abstract

The growing importance of the planetary boundary layer (PBL) height detection is apparent in various fields, from air pollution analysis to weather prediction. Here, we demonstrate the capability of ceilometers to serve as a validation tool for the models' PBL height estimations. The study focused on the daytime summer PBL heights over a heterogeneous area. Height values from two numerical weather models, the global IFS model, and the regional COSMO model were evaluated against actual measurements from a radiosonde and eight ceilometers. The evaluation of the PBL heights was attained by the bulk Richardson method and the parcel method. The ceilometers' backscatter profiles were analyzed by the wavelet covariance transform method. A comparison of the PBL heights at 11 UTC on 33 summer days in Beit Dagan radiosonde launch site revealed a good agreement between the radiosonde and the adjacent ceilometer (mean error = 12 m, RMSE = 97 m). Spatial analysis on 13 days compared to results from five ceilometer sites showed COSMO evaluations by the bulk Richardson method ($COSMO_R$) produced good results for both flat (mean error = 19 m, RMSE = 203 m) and elevated terrain (mean error = -6 m, RMSE = 251 m). To correct $COSMO_R$ height estimations, a regression tool was generated based on the PBL height difference between $COSMO_R$ and eight ceilometers from diverse sites. The independent predictor variables are the topography and the distance from the shoreline. The correction factors are implemented on the $COSMO_R$ PBL height results.

1. Introduction

In this era of heavy industrialization, the need to mitigate the detrimental effects of air pollution exposure is unquestionable. However, in order to regulate and establish environmental thresholds, a comprehensive understanding of the air pollution dispersion processes is necessary. One of the key meteorological parameters governing air pollution dispersion is the planetary boundary layer (PBL) height. The PBL height is classified as the first level of the atmosphere which dictates the vertical dispersion extent of air pollution (Stull, 1988). Consequently, the concentration level of air pollution varies depending on the height of the PBL.

Applicable evaluation of PBL heights can be derived either by actual measurements or estimations based on numerical weather prediction (NWP) models. On the one hand, NWP models, such as regional models, provide high temporal and spatial data resolution beyond the capability of actual measurements. On the other, they are based on mathematical equations with initial assumptions and boundary conditioned set beforehand. Hence, the models' products require a systematic validation tool based on actual measurements.

There are two main PBL height measurement methods: in-situ radiosonde launches and remote sensing such as lidars and profilers. Unfortunately, radiosonde launches are costly as successive measurements. Profilers and sophisticated lidars produce high temporal resolution profiles but are limited in space. Moreover, certain meteorological conditions may reduce their performance, such as precipitation for radio acoustic sounding system profilers (Uzan et al., 2012) and dust storms for Raman lidars (Mamouri et al., 2016).

These limitations have led several research groups to successfully utilized ceilometers - single wavelength cloud base height detectors, as a means to recognize and determine the PBL height (Eresmaa et al., 2006, Haeffelin and Angelini, 2012, Wiegner et al., 2014). Ubiquitous in airports and meteorological service centers worldwide, ceilometers obtain a wide spatial resolution per lidar (for further information see TOPROF of COST Action ES1303 and E-PROFILE of the EUMETNET Profiling Program). They produce high temporal resolution profiles about every 15 s and every 10 m, up to several km, retrieved as attenuated backscatter signals. The ceilometers are low cost, easy to maintain, and operate continuously unattended under diverse meteorological conditions (Kotthaus and Grimmond, 2018). These qualities reflect their advantages over high-cost, multi-wavelength sophisticated lidars, that require surveillance, calibration procedures, and careful maintenance. Hence, they are limited in space

and operational time (Mamouri et al., 2016) and cannot achieve the spatial and temporal measurements coverage essential to validate the PBL heights generated by NWP models.

Gierens et al (2018) established a PBL height algorithm applied to the ceilometers' profiles. The PBL height was classified according to daytime convective mixing and nighttime stable surface layer accompanied by a residual layer aloft. Their research was conducted in northwestern South Africa from October 2012–August 2014, showed good agreement with ERA-Interim reanalysis.

Another operational PBL height detection method was established by Collaud Coen et al. (2014). Their study, implemented on a two-year data set for two rural sites located on the Swiss plateau, included several remote sensing instruments (wind profiler, Raman lidar, microwave radiometer) and several algorithms (the parcel method, the bulk Richardson number method, surface-based temperature inversion, and aerosol or humidity gradient analysis). The results were validated against radio-sounding measurements and compared to the NWP model COSMO-2 (2.2 km resolution). In this research, the authors recommended using ceilometers as complementary measurements of the residual layer.

Ketterer et al. (2014) focused on the development of the PBL in the Swiss Alps by an adjacent ceilometer, wind profiler, and in-situ continuous aerosol measurements. The ceilometer's profiles were analyzed by the gradient and STRAT-2D algorithms. Good agreement was found between the PBL height derived from the ceilometer and wind profiler during the daytime and under cloud-free conditions. However, comparisons to the calculated PBL heights from the COSMO-2 model yielded low correlations.

Despite this extensive research, so far, scarce attention has been paid to designate ceilometers as a correction tool for NWP PBL height assessments. The main goal of this study was to evaluate the estimations of the models for the daytime summer PBL heights over complex terrain by comparing the results against remote sensing measurements from ceilometers. Ceilometers produce aerosol backscatter profiles, therefore, the evaluation of the PBL height during precipitation episodes becomes difficult (Collaud et al. 2014, Ketterer et al. 2014, Kotthaus & Grimmond 2018). Accordingly, this study focused on the summer season.

The research area and time period are explained in Sect. 2. The models and instruments applied are described in Sect. 3 and Sect. 4, respectively. The PBL height detection methods are presented in Sect. 5. Results of NWP models compared to in-situ radiosonde and ceilometer measurements are presented in Sect. 6. Finally, summary and conclusions are drawn in Sect. 7

regarding the capabilities of NWP models and the evolution of the daytime summer PBL height over Israel.

2. Research area

Located in the East Mediterranean, Israel obtains a heterogeneous research area in comparatively short distances, comprised of mountains and valleys in the north and the east, a coastline in the west and a desert in the south. This provides a range of meteorological conditions, from the humid climate on the coast to the arid south.

The Israeli summer season (June-September) is characterized by dry weather (no precipitation), high relative humidity (RH) - up to 80% in midday in the shoreline (Israeli Meteorological Service -IMS weather reports) and sporadic shallow cumulus clouds. On the synoptic scale, the summer is defined by a persistent Persian Trough (either deep, shallow or medium) followed by a Subtropical High aloft (Felix Y., 1994, Dayan et al., 2002, Alpert et al., 2004). Combined with the sea breeze, the average PBL height is found to be quite low. For example, the average summer PBL height in Beit Dagan (33 m a.s.l and 7.5 km east from the shoreline) reaches ~900 m a.g.l after sunrise, and before the entrance of the sea breeze front (Felix Y.,1994, Dayan and Rodinzki, 1999, Uzan et al., 2016, Yuval et al., 2019). Summer dust outbreaks in the eastern Mediterranean are quite rare (Alpert and Ziv 1989, Alpert et al., 2000) therefore, they were not addressed here, especially in the height levels below 1 km (Alpert et al., 2002).

Previous research describes the formation and evolution of the Israeli summer PBL height as a function of the synoptic and mesoscale conditions, as well as the distance from the shoreline, and the topography. Overall, the diurnal PBL height in the summer season may be portrayed in the following manner: After sunrise (~4-5 LST, where LST=UTC+2) clouds initially formed over the Mediterranean Sea are advected eastward to the shoreline. As the ground warms up, the nocturnal surface boundary layer (SBL) dissipates and buoyancy induced convective updrafts instigate the formation of the sea breeze circulation (Stull, 1988). The entrance of the sea breeze front (SBF) is estimated between 7-9 LST (Felix Y., 1993, Alpert and Rabinovich-Hadar, 2003, Uzan and Alpert, 2012), depending on the time of sunrise and the different synoptic modes of the prevailing system – the Persian Trough (Alpert et al., 2004). Cool and humid marine air hinder the convective updrafts. Clouds dissolve and the height of the shoreline convective boundary layer (CBL) lowers by ~250 m (Felix Y., 1993, Felix Y., 1994,

Levi et al., 2011, Uzan and Alpert, 2012). Further inland, the convective thermals continue to inflate the CBL (Hashmonay et al., 1991, Felix, 1993, Lieman, R. and Alpert, 1993). The sea breeze circulation steers clockwise and the PBL wind speed is enhanced by the west-north-west synoptic winds (Neumann, 1952, Neumann, 1977, Uzan and Alpert, 2012). By noontime (~11-13 LST) maximum wind speeds further suppress the CBL (Uzan and Alpert, 2012). In the afternoon (~13-14 LST), the SBF reaches ~30-50 km inland to the eastern elevated complex terrain (Hashmonay et al., 1991, Lieman, R. and Alpert, 1993). At sunset (~18-19 LST), as the insolation diminishes, the potential energy of the convective updrafts weakens and the CBL height drops (Dayan and Rodnizki, 1999). After sunset, the CBL finally collapses and a residual layer (RL) is formed above the SBL (Stull, 1988) as the ground cools down. High humidity and low RL create low condensation levels and shallow evening clouds are produced.

3. IFS and COSMO Models

The IMS utilizes two operational models: The European Centre for Medium-range Weather Forecasts (ECMWF) Integrated Forecast System (IFS) global model, and the consortium for small-scale modeling (COSMO) regional model. Details of each model are given in Table 2.

COSMO (~2.5km resolution) has been running at the IMS over the Eastern Mediterranean domain (25-39 E/26-36 N) since 2013, with boundary and initial conditions from IFS. It is based on the primitive thermo-hydrodynamic equations describing non-hydrostatic compressible flow in a moist atmosphere (Steppeler et al., 2003, Doms et al., 2011, Baldauf et al., 2011). Its vertical extension reaches 23.5 km (~30 hPa) with 60 vertical levels. The model runs a two-time level integration scheme based on a third order of the Runge–Kutta method and a fifth-order of the upwind scheme for horizontal advection. Unlike IFS, the deep convection parametrization is switched off, while only the shallow convection is parameterized (Tiedtke, 1989). The turbulence scheme, based on Mellor and Yamada (1982) at Level 2.5, uses a reduced second-order closure with a prognostic equation for the turbulent kinetic energy. The transport and local time tendency terms in all the other second-order momentum equations are neglected and the vertical turbulent fluxes are derived diagnostically (Cerenzia I., 2017).

The resolution of IFS has improved from ~13 km in 2015 to ~10 km in 2016 and consists of 137 vertical levels. Its turbulent diffusion scheme represents the vertical exchange of heat, momentum, and moisture through sub-grid scale turbulence. In the surface layer, the turbulence fluxes are computed using a first-order K-diffusion closure based on the Monin-Obukhov (MO)

similarity theory. Above the surface layer, a K-diffusion turbulence closure is used everywhere except for unstable boundary layers where an Eddy-Diffusivity Mass-Flux (EDMF) framework is applied to represent the non-local boundary layer eddy fluxes (Koehler et al. 2011).

The spatial resolution of the models affects their ability to refer to the actual topography rather than a smoothed grid point. Therefore, the models' results were corrected by the actual ground base heights for each measurement site (Table 1).

Concerning the time resolution, IFS produced hourly results while COSMO generated profiles every 15 min. To compare PBL heights from both models, a series of trials disclosed that COSMO profiles of the last 15 min within an hour best represent the hourly values of IFS.

4. Instruments

4.1 Ceilometers

Vaisala ceilometers type CL31, commonly deployed worldwide, are the main research tool in this study. CL31 is a pulsed, elastic micro-lidar, employing an Indium Gallium Arsenide (InGaAs) laser diode transmitter of a near-infrared wavelength of 910 nm ±10 nm at 25˚C with a high pulse repetition rate of 10 kHz every two seconds (Vaisala ceilometer CL31 user's guide: http://www.vaisala.com). The backscatter signals are collected by an avalanche photodiode (APD) receiver and designed as attenuated backscatter profiles at intervals of 2-120 s (determined by the user). In this study, CL31 ceilometers were applied with the exception of ceilometer CL51 in the Weizmann Institute (Fig.1, Table 1). CL51 consists of a higher signal and signal-to-noise ratio, hence the backscatter profile measurement reaches up to 15.4 km compared to 7 km of CL31.

One drawback is that calibration procedures were nonexistent in all sites, and in most cases, maintenance procedures (cleaning of the ceilometer window) were not regularly carried out, with the exception of the IMS Beit Dagan ceilometer. Nevertheless, the PBL height detection is based on a pronounced change of the attenuated backscatter profile. This change is attributed to variations in the aerosol content providing indications for both clouds and atmospheric layers. Therefore, the limitation of a single wavelength within the spectral range of water vapor absorption does not affect this type of detection. In order to derive the backscatter coefficient from ceilometer measurements, signal calibrations and water vapor corrections are necessary (Weigner et al., 2014, Wiegner and Gasteiger, 2015).

The ceilometers produce profiles every 15 or 16 sec (Table 1). In order to compare them to the models' hourly results (Sect. 3), they were averaged to half-hour ones, whereas the second half-hour profile within each hour was chosen for the comparison process.

The nocturnal SBL heights in ground-level ceilometer sites were detected mainly within the ceilometers' first range gates. At these heights, a constant perturbation existed due to the overlap of the emitted laser beam and the receiver's field of view. This fact limited our capability to determine the low SBL height of the summer season and heightened our decision to focused on daytime CBL heights. Detailed information regarding the manufactural and technical properties of ceilometers involved in this research are given in Uzan et al. (2018).

4.2 Radiosonde

The IMS obtains systematic radiosonde atmospheric observations twice daily, at 23 UTC and 11 UTC, adjacent to a ceilometer. Launching is performed in Beit Dagan (32.0 ° long, 34.8 ° lat, 33 m a.s.l), situated 7.5 km east from the shoreline, 11 km southeast to Tel Aviv, 45 km northwest to Jerusalem (Fig.1 and Table 1). The radiosonde, type Vaisala RS41-SG, produces profiles of RH, temperature, pressure, wind speed and wind direction as it ascends. Measurements are retrieved every 10 seconds, corresponding to about every 45 m, reaching 2 km in about 8 minutes. The horizontal displacement of the radiosonde depends on the intensity of the ambient wind speed. The average wind speed along the 11 UTC summer profiles is about 5 m/s (Uzan et al., 2012). Therefore, the horizontal displacement of the radiosonde from its launch position is fairly low and is estimated at about 2.5 km. Moreover, the radiosonde position resolution is defined as 0.01°. As aforementioned, the PBL height in Beit Dagan for midday summer is estimated below 1 km (Dayan and Rodinzki, 1999, Uzan et al., 2016, Yuval et al., 2019). Hence, within an ascending height of 1 km, the change in the radiosonde's horizontal position is under 0.01° which is an order of magnitude from the models' grid resolution. Thus, we assert the radiosonde profiles represent the Beit Dagan site and the displacement error of the ascending radiosonde can be neglected.

5. Methods

5.1 The bulk Richardson number method

COSMO and IFS schemes calculate the PBL height by the bulk Richardson number method (R_b) as the most reliable technique for PBL height detection by NWP models (Zhang et al., 2014).

The bulk Richardson number formula (Hanna R. Steven,1969, Zhang et al., 2014) is given in the following manner:

$$R_b = \frac{\frac{g}{\theta_v}(\theta_{vz}-\theta_{v0})(Z-Z_0)}{U^2+V^2} \quad (1)$$

where g is the gravitational force, θ_{vz} is the virtual potential temperature at height Z, θ_{v0} is the virtual potential temperature at ground level (Z_0). U and V are the horizontal wind speed components at height Z.

The IFS model defines the PBL height as the lowest height level at which the R_b (Eq. 1) reaches a critical threshold of 0.25 (ECMWF-IFS documentation – Cy43r3, Part IV: Physical Processes, July 2017). The PBL height is distinguished by scanning the bulk Richardson values from the surface level upwards. If the PBL height is found between two levels of the model, it is determined by linear interpolation.

Radiosonde's profiles were analyzed in the same manner by a R_b threshold of 0.25 to detect a specific height rather than a certain layer.

COSMO estimates the R_b based on the dynamic conditions of the first four levels (10, 34.2, 67.9, 112.3 m a.g.l.) signified by a threshold of 0.33 for stable conditions and 0.22 for unstable ones. If no level is found, then a missing value is assigned for the PBL height.

5.2 The parcel method

The PBL height is defined by the parcel method as the height aloft at which the value of the virtual potential temperature reaches that of the surface level (Holzworth 1964, Stull, 1988, Seidel et al., 2010). The calculation of the virtual potential temperature is as follows:

$$\theta_v = T_v \left(\frac{P_0}{P}\right)^{\frac{Rd}{Cp}} \quad (2)$$

where P_0 is the ground level atmospheric pressure, P is the at atmospheric pressure at height Z, R_d is the gas constant of dry air, C_p is the heat capacity of dry air in a constant pressure ($\frac{R_d}{C_p}$ = 0.286). The virtual temperature (T_v) is obtained by:

$$T_v = \frac{T}{1-\frac{e}{P}(1-\varepsilon)} \quad (3)$$

where T is the temperature at height Z, e is the actual vapor pressure and ε is the ratio of the gas constant of air and water vapor (ε=0.622). The actual vapor pressure (e) is derived by the relative humidity (RH) profile multiplied by the saturated vapor pressure (e_s). The saturated vapor pressure was derived by the temperature profile.

In this method, the value of the virtual potential temperature at surface height is crucial. The first levels of IFS and COSMO are 10 m a.g.l and 20 m a.g.l, respectively. Thus, evaluations of the ambient temperature and the dew point temperature (or RH) for 2 m a.g.l are generated by the models based on the similarity theory.

5.3 The wavelet covariance transform method

The wavelet covariance transform (WCT) method is operated along the length of the backscatter profile (Brooks Ian, 2003). This method is based on the Haar step function (Baars et al., 2012) given in Eq. (4) and Eq. (5) as follows:

$$W_{f(a,b)} = \frac{1}{a}\int_{Zb}^{Zt} f(z)h\left(\frac{z-b}{a}\right)dz \quad (4)$$

where $W_{f(a,b)}$ is the local maximum of the backscatter profile ($f(z)$) determined within the range of step (a). The length of the step is the number of height levels (n) multiplied by the profile height resolution (Δz) from ground level (Zb) and up (Zt).

The Haar step function, given in Eq. (5), is equivalent to a derivative at height z, representing the value difference of each step (a) above and beneath a point of interest (b). Here, b is the

measurement heights of the ceilometer along the profile (every 10 m starting from 10 m a.g.l) and step a was defined as 20 m (10 m above and beneath point b).

$$h\left(\frac{z-b}{a}\right) = \begin{cases} +1, & b - \frac{a}{2} \le z \le b, \\ -1, & b \le z \le b + \frac{a}{2} \\ 0, & elsewhere \end{cases} \quad (5)$$

To evaluate the ceilometers' PBL heights (Eq. 4), the backscatter profiles are analyzed by the WCT method between two boundaries. The lower boundary (Zb) is the height above the perturbation of the overlap function (~ 100 m, see Sect. 4.1). The upper limit (Zt) is either the height point with the largest variance within a step or the first height point with negative values indicating a low signal-to-noise ratio. The lowest height among the two aforementioned options will define the upper limit.

When clouds exist (mainly shallow cumulus clouds), the algorithm defines the PBL height as the highest measurement point of the cloud above the cloud base height. This height indicates the entrainment zone rather than the actual cloud top.

6. Results

6.1 Comparison to in-situ radiosonde profiles

In order to evaluate the daytime PBL heights produced by the models and the ceilometers, the results were compared to the radiosonde's evaluations. Consequently, the investigation was held in Beit Dagan launch site at the time of the midday launch (11 UTC). For this comparison, the ceilometer's 15 s profiles were averaged as half-hour profiles between 10:30-11:00 UTC. COSMO's results referred to the profiles of 10:45 UTC, and IFS estimations were given at 11 UTC. The analysis was carried out for 33 summer days, 13 days from August 2015, and 20 days from Aug 2016. The PBL heights were produced by the same methods: the parcel method (denoted by subscript P) and the bulk Richardson method (denoted by subscript R). These methods require meteorological parameters such as temperature and pressure profiles generated by the models and the radiosonde. Ceilometers, on the other hand, produce only backscatter signals. Therefore, they were analyzed by the WCT method. The results were statistically analyzed by mean error (ME), root mean square error (RMSE), and correlation (R) presented in Fig. 2 and Table 3.

Good agreement was found between the ceilometer and the radiosonde (ME = 12 m, RMSE = 97 m, and R = 0.93), although they produced the PBL heights by different methods. Among the models and methods, $COSMO_R$ retrieved the best results of ME = -3 m, RMSE = 152 m and R = 0.83). IFS predominantly overestimated the PBL heights. The poorest results were generated by IFS_R (ME = 274 m, RMSE = 432 m, R = 0.18).

An example of an analysis on a typical day is given in Fig. 3 for August 15, 2015. On this day, the PBL height at 11 UTC was estimated at 680 m a.s.l by the radiosonde. $COSMO_P$ accurately estimated the same height while $COSMO_R$ detected the height to be 100 m lower (580 m a.s.l). The ceilometer overestimated by 100 m (795 m a.s.l). IFS results were twice the value produced by the radiosonde (IFS_R=1,300 m a.s.l, IFS_P= 1,474 m a.s.l).

Among the 33 days tested, the largest gap was found between IFS_R and RS_R on August 17, 2016 (Fig. 2). The imprecision could be due to the fact that the Richardson method is based solely on dry thermodynamics for local turbulence (Von Engeln and Teixeira, 2013), while on August 17, 2016, the 11 UTC PBL height was determined through a multi-layer cloud (not shown).

6.2 Spatial analysis by ceilometers

After the good results generated by the WCT method imposed on the ceilometer's profiles, ceilometers were applied as PBL height detectors in sited where no other atmospheric measurements operated. The same analysis process was carried out but for five ceilometer sites (Ramat David, Tel Aviv, Beit Dagan, Weizmann, and Jerusalem), representing diverse terrain on 13 specific days available from all instruments and models. This time the models' results were compared to the ceilometers' measurements in each site. Both models defined the Tel Aviv site by a grid point mostly over the Mediterranean Sea. Therefore, we shifted the Tel Aviv coordinates to an adjacent grid point that was mostly land, representing Tel Aviv by the same height and distance from the shoreline.

A comparison to radiosonde's results was available only in Beit Dagan. Figure 4b reveals a good agreement between the radiosonde and the ceilometer's evaluations in Beit Dagan, although the different methods imposed on each instrument. A significant case on August 10, 2015, where an atmospheric layer above the PBL height denoted by the radiosonde and the ceilometer (not shown) led to the models' discrepancies.

By and large, $COSMO_R$ achieved the best statistical results (Tables 4-5) regarding flat and complex terrain, of RMSE from 175 m in Weizmann (60 m a.s.l, and 11.5 km east from the shoreline) up to 251 m in Jerusalem (830 m a.s.l and 53 km east from the shoreline), and ME between 19 m in Tel Aviv (5 m a.s.l, and 50 m from shoreline), and -26 m in Ramat David (50 m a.s.l, and 24 km east from the shoreline). IFS_P produced high RMSE results starting at 180 m in Ramat David rising up to 569 m in Beit Dagan, and ME up to 497 m in Beit Dagan. These results emphasize the advantage of high-resolution regional models such as COSMO (~2.5 km resolution) over the IFS global model (resolution of ~13 km in 2015 and ~10 km in 2016) over a diverse area.

6.3 COSMO PBL height correction

Finally, the spatial daytime summer PBL heights were investigated. Following the conclusions of previous stages, $COSMO_R$ was chosen as the model and method that achieved the best results. Average hourly values were derived between 09-14 UTC (corresponding to 11 -16 LST) and compared to the results from eight ceilometer sites (Fig. 1, Table 1). The comparison was accomplished by all dates available for each ceilometer site on August 2015: Jerusalem - 21 days, Nevatim - 13 days, Hazerim - 20 days, Ramat David - 26 days, Weizmann - 25 days, Beit Dagan - 13 days, Hadera - 16 days, Tel Aviv - 25 days.

In order to validate and correct $COSMO_R$ results by the ceilometers' measurements, a correction tool based on a regression function was implemented for each hour (09-14 UTC), for all ceilometers' sites simultaneously by the following formula:

$$ME_{st} = \alpha G + \beta D + \gamma \quad (6)$$

where ME_{st} is the dependent variable representing the PBL height mean error for each ceilometer station (st) compared to the results obtained by the $COSMO_R$. The independent predictor variables are the ground altitude of the ceilometer's site (G) and its distance from the shoreline (D). The correction factors α, β, and γ are implemented on the $COSMO_R$ PBL height results.

$COSMO_R$ mean PBL heights cross-section from Tel Aviv (34.8° lat) to Jerusalem (35.2° lat) is presented in Fig. 5. Before the correction (Fig. 5a), $COSMO_R$ approximated Tel Aviv PBL heights descend gradually from 750 at 09 UTC (11 LST) to 600 m a.s.l at 14 UTC (16 LST). Apparently, the correction tool reduced the height difference to ~700 m a.s.l with the exception

of ~750 m a.s.l at 09 UTC (Fig. 5b). These results correspond to Uzan et al, (2012) showing Tel Aviv site is practically on the shoreline, therefore as the sea breeze enters Tel Aviv (~ 08 UTC), it surmounts the convective thermals preventing from the mixed layer to inflate.

In Jerusalem, the summer PBL height inflates according to the insolation intensity, as the main source of the buoyancy force. Therefore, the maximum daytime PBL heights are measured at midday. In the afternoon, when the sea breeze reaches eastern Israel, the height decreases. $COSMO_R$ results before and after the correction showed the highest value at 11 UTC (13 LST), corresponding to maximum insolation at midday. The lowest value was corrected from 09 UTC (11 LST) to 14 UTC (16 LST) as insolation decreases and the cool and humid air of sea breeze front demolishes the thermals and the PBL height subsides.

Between the shoreline of Tel Aviv and the eastern mountains of Jerusalem, the overall range of PBL height values was reduced. For example, in 35° lat (between Weizmann - 60 m a.s.l and Jerusalem - 830 m a.s.l), the PBL heights of 09-14 UTC varied from 750 to 1500 m a.s.l. After the correction, the height values ranged from 1000 to 1400 m a.s.l, generating higher PBL heights for the daytime hours. Fig. 6 demonstrated the correction tool at 14 UTC disclosing a correction of ~ 300 m (Fig. 6b) over the complex terrain of Jerusalem (830 m a.s.l) and Nevatim (400 m a.s.l).

7. Summary and Conclusions

Earlier studies have successfully employed ceilometers for PBL height detection, typically under dry conditions. However, these studies employed weather models primarily as a validation tool rather than investigating the models' predictive capabilities. Here, we tested the ability of ceilometers to serve as a correction tool for PBL height estimations derived from two operational models: the IFS global model, and the mesoscale COSMO regional model. The study focused on the daytime summer PBL heights.

Firstly, we compared the models' and the ceilometer's evaluations to actual measurements from an adjacent radiosonde in the Beit Dagan launch site. Results for 11 UTC on 33 August days revealed the promising ability of the WCT method to detect the PBL heights generated by the radiosonde by the bulk Richardson method and by the parcel method (RMSE= 97 m).

In the next stage, the investigation expanded spatially to four other diverse measuring sites, from the shoreline of Tel Aviv (5 m a.s.l) to the mountainous Jerusalem (830 m a.s.l). The same

methods were applied for 13 summer days, except this time, the models' values were compared to the ceilometers' measurements in each site. The results disclosed the COSMO model based on the bulk Richardson method ($COSMO_R$) achieved the best results for both flat (Tel Aviv: RMSE=203 m, ME=19 m) and complex terrain (Jerusalem: RMSE = 251m, ME = -6 m).

Finally, the temporal and spatial evolution of the summer daytime (11-16 LST) PBL heights were examined. The heights were derived by $COSMO_R$ and compared to ceilometers measurements distributed in eight sites across Israel, providing a heterogeneous research area in comparatively short distances. A correction tool was established based on a regression function comprised of the topography of the ceilometer's site (G) and its distance from the shoreline (D) serving as the independent predictor variables. The results revealed corrections up to ~ 300 m difference which improved the description of the diurnal PBL heights.

Despite the limited database, our results offer a preview of the great potential of ceilometers as a validation and a correction tool to discern PBL heights derived from weather models. Future research should, therefore, include a larger dataset to evaluate whether these results are retained in the long term and to define a systematic validation process.

Data availability

Weather reports- Israeli Meteorological Service weather reports (in Hebrew): http://www.ims.gov.il/IMS/CLIMATE/ClimateSummary.

Radiosonde profiles – Israeli Meteorological Service provided by request.

Ceilometer profiles - the data is owned by governmental offices and provided by request.

Author contribution

Leenes Uzan carried out the research and prepared the manuscript under the careful guidance of Pinhas Alpert and Smadar Egert alongside a fruitful collaboration with Yoav Levi, Pavel Khain and Elyakom Vladislavsky. The authors declare that they have no conflict of interest.

Acknowledgments

We wish to thank the Israeli Meteorological Service, the Israeli Air Force, the Association of Towns for Environmental Protection (Sharon-Carmel), and Rafat Qubaj from the Department of Earth and Planetary Sciences at the Weizmann Institute of Science, for their ceilometer data. We are indebted to Hadas Marcus for her editing assistance.

References

Alpert P., and Ziv B.: The Sharav cyclone observations and some theoretical considerations, J. Geophys. Res., 94, 18495–18514, 1989.

Alpert P., Herman J., Kaufman Y. J., and Carmona I.: Response of the climatic temperature to dust forcing, inferred from TOMS Aerosol Index and the NASA assimilation model. J. Atmos. Res., 53, 3-14, 2000.

Alpert, P., Krichak, S. O., Tsidulko, M., Shafir, H., and Joseph, J. H.: A Dust Prediction System with TOMS Initialization, Mon. Weather Rev., 130, 2335–2345, 2002.

Alpert P., and Rabinovich-Hadar M.: Pre- and post-frontal lines - A meso gamma scale analysis over south Israel, J. Atmos. Sci., 60, 2994-3008, 2003.

Alpert, P., Osetinsky, I., Ziv, B., Shafir H.: Semi-objective classification for daily synoptic systems: Application to the eastern Mediterranean climate change. Int. J. of Climatol., 24, 1001-1011, 2004.

Baars, H., Ansmann, A., Engelmann, R., and Althausen, D.: Continuous monitoring of the boundary layer top with lidar, Atmos. Chem. Phys., 8, 7281–7296, https:// doi:10.5194/acp-8-7281-2008, 2008.

Baldauf, M., A. Seifert, J. Förstner, D. Majewski, M. Raschendorfer, and T. Reinhardt: Operational Convective-Scale Numerical Weather Prediction with the COSMO Model: Description and Sensitivities. Mon. Wea. Rev., 139, 3887–3905, https://doi.org/10.1175/MWR-D-10-05013.1, 2001.

Bechtold, P.: Convection parametrization. ECMWF Seminar proceedings on "The parametrization of subgrid physical processes", 63-85, 2008.

Brooks, I.: Finding Boundary Layer Top: Application of a wavelet covariance transform to lidar backscatter profiles, J. Atmos. Ocean. Tech., 20, 1092–1105, 2003.

Cerenzia I., Challenges and critical aspects in stable boundary layer representation in numerical weather prediction modeling: diagnostic analyses and proposals for improvement, Ph.D. thesis, University of Bologna, 2017.

Collaud Coen, M., Praz, C., Haefele, A., Ruffieux, D., Kaufmann, P., and Calpini, B.: Determination and climatology of the planetary boundary layer height above the Swiss plateau

by in situ and remote sensing measurements as well as by the COSMO-2 model, Atmos. Chem. Phys., 14, 13205-13221, https://doi.org/10.5194/acp-14-13205-2014, 2014.

Dayan, U., Shenhav, R., Graber, M.: The Spatial and temporal behavior of the mixed layer in Israel, J Appl Meteorol, 27, 1382- 1394, 1988.

Dayan, U., Rodnizki, J.: The temporal behavior of the atmospheric boundary layer in Israel. J Appl Meteorol, 38, 830-836, 1999.

Dayan, U., Lifshitz-Goldreich B., and Pick, K.: Spatial and structural variation of the atmospheric boundary layer during summer in Israel-Profiler and rawinsonde measurements. J. Appl. Meteor., 41, 447-457,2002.

Doms, G., J. Förstner, E. Heise, H.-J. Herzog, D. Mironov, M. Raschendorfer, T. Reinhardt, B. Ritter, R. Schrodin, J.-P. Schulz, and G. Vogel: A description of the nonhydrostatic regional COSMO model. Part II: Physical parameterization. Deutscher Wetterdienst, Ofenbach, 154 pp, 2011.

Eresmaa, N., Karppinen, A., Joffre, S. M., Räsänen, J., and Talvitie, H.: Mixing height determination by ceilometer, Atmos. Chem. Phys., 6, 1485-1493, https://doi.org/10.5194/acp-6-1485-2006, 2006.

Feliks, Y.: A numerical model for estimation of the diurnal fluctuation of the inversion height due to a sea breeze, Bound. Layer Meteor., 62, 151-161. 1993.

Feliks, Y: An analytical model of the diurnal oscillation of the inversion base due to sea breeze, J. Atmos. Sci., 51, 991-998,1994.

Feliks, Y: Nonlinear dynamics and chaos in the sea and land breeze, J. Atmos. Sci., 61, 2169-2187, 2004.

Gierens, R.T., Henriksson, S., Josipovic, M., Vakkari, V., Van Zyl, P.G., Beukes J.P., Wood, C.R., O'Connor, E.J.: Observing continental boundary layer structure and evolution over the South African savannah using a ceilometer, Theor. Appl. Climatoi., 136, 333-346, https://doi.org/10.1007/s00704-018-2484-7, 2018.

Haeffelin, M. and Angelini, F.: Evaluation of mixing height retrievals from automatic profiling lidars and ceilometers in view of future integrated networks in Europe, Bound. Lay. Meteorol., 143, 49–75, 2012.

Hanna, S. R.: The thickness of the planetary boundary layer, Atmos. Environ., 3, 519–536, 1969.

Hashmonay, R., Cohen, A., and Dayan, U.: Lidar observations of the atmospheric boundary layer in Jerusalem, J. Appl. Meteorol, 30, 1228-1236, 1991.

Holzworth, C. G.: Estimates of mean maximum mixing depths in the contiguous United States, Mon. Weather Rev., 92, 235–242, 1964.

Ketterer, C., Zieger, P., Bukowiecki, N.: Bound. Lay. Meteo., 151, 317-334, https://doi.org/10.1007/s10546-013-9897-8, 2014.

Koehler, M., Ahlgrimm, M. and Beljaars, A.: Unified treatment of dry convective and stratocumulus-topped boundary layers in the ECMWF model, Q. J. R. Meteorol. Soc., 137, 43-57, 2011.

Kotthaus, S. and Grimmond, C.S.B.: Atmospheric boundary-layer characteristics from ceilometer measurements. Part 1: a new method to track mixed layer height and classify clouds, Q J R Meteorol. Soc.,144 (714), 1525–1538, https://doi.org/10.1002/qj.3299, 2018.

Levi Y., Shilo E., and Setter I.: Climatology of a summer coastal boundary layer with 1290-MHz wind profiler radar and a WRF simulation, J. Appl. Meteorol. Climatol., 50, 1815-1826, https://doi.org/10.1175/2011JAMC2598.1, 2011.

Lieman, R. and Alpert, P.: Investigation of the planetary boundary layer height variations over complex terrain, Bound. Lay. Meteorol., 62, 129-142, 1993.

Mamouri, R.E., Ansmann, A., Nisantzi, A., Solomos, S., Kallos, G., and Hadjimitsis, D.G.: Extreme dust storm over the Eastern Mediterranean in September 2015: satellite, lidar, and surface observations in the Cyprus region, Atmos. Chem. Phys., 16(21), 13711-13724, 2016.

Neumann J.: Diurnal variations of the subsidence inversion and associated radio wave propagation phenomena over the coastal area of Israel. Isr. Met. Serv, 1952.

Neumann J.: On the rotation rate of the direction of sea and land breezes. J. Atmos. Sci., 34, 1913-1917, 1977.

Seidel, D. J., Ao, C. O., and Li, K.: Estimating climatological planetary boundary layer heights from radiosonde observations: Comparison of methods and uncertainty analysis, J. Geophys. Res., 115, D16113, doi:10.1029/2009JD013680, 2010.

Steppeler J., Doms G., Schattler U., Bitzer HW, Gassmann A., Damrath U., Gregoric G.: Meso gamma scale forecasts by nonhydrostatic model LM. Meteorological Atmospheric Physics, 82, 75–96, 2003.

Stull R.B.: An introduction to boundary layer meteorology, Kluwer Academic Publishers, the Netherlands, 666 p., 1988.

Tiedtke, M., 1989: A Comprehensive Mass Flux Scheme for Cumulus Parameterization in Large-Scale Models. Mon. Wea. Rev., 117, 1779–1800, https://doi.org/10.1175/1520-0493, 1989.

Uzan, L. and Alpert, P.: The coastal boundary layer and air pollution - a high temporal resolution analysis in the East Mediterranean Coast, The Open Atmospheric Science Journal, 6, 9–18, 2012.

Uzan, L., Egert, S., and Alpert, P.: Ceilometer evaluation of the eastern Mediterranean summer boundary layer height – first study of two Israeli sites, Atmos. Meas. Tech., 9, 4387–4398, https://doi.org/10.5194/amt-9-4387-2016, 2016.

Von Engeln A., and Teixeira J.: A planetary boundary layer height climatology derived from ECMWF reanalysis data. J. Climate., 126, 6575-6590, https://doi.org/10.1175/JCLI-D-12-00385, 2013.

Wiegner M., Madonna F., Binietoglou I., Forkel R., Gasteiger J., Geiß A., Pappalardo G., Schäfer K., and Thomas W.: What is the benefit of ceilometers for aerosol remote sensing? An answer from EARLINET, Atmos. Meas. Tech., 7, 1979–1997, https://doi.org/10.5194/amt-7-1979-2014, 2014.

Wiegner, M. and Gasteiger, J.: Correction of water vapor absorption for aerosol remote sensing with ceilometers, Atmos. Meas. Tech., 8, 3971–3984, https://doi.org/10.5194/amt-8-3971-2015, 2015.

Yuval, Dayan, U., Levy, I., & Broday, D. M: On the association between characteristics of the atmospheric boundary layer and air pollution concentrations, Atmospheric Research, doi.org/10.1016/j.atmosers.2019.104675, 2019.

Zhang, Y., Gao, Z., Li, D., Li, Y., Zhang, N., Zhao, X., and Chen, J.: On the computation of planetary boundary-layer height using the bulk Richardson number method, Geosci. Model Dev., 7, 2599-2611, https://doi.org/10.5194/gmd-7-2599-2014, 2014.

Table 1. Location of measurements sites and ceilometer types

Location	Site	Long/Lat	Distance from shoreline (km)	Height (m a.s.l)	Ceilometer type (resolution, height limit[a])
Ramat David (RD)	North	32.7 °/35.2 °	24	50	CL31 (10 m,16 s, up to 7.7 km)
Hadera (HD)	Shoreline	32.5 °/34.9 °	3.5	10	CL31 (10 m,16 s, up to 7.7 km)
Tel Aviv (TLV)	Shoreline	32.1 °/34.8 °	0.05	5	CL31 (10 m,16 s, up to 7.7 km)
Beit Dagan (BD)[b]	Inland	32.0 °/34.8 °	7.5	33	CL31 (10 m,15 s, up to 7.7 km)
Weizmann (WZ)	Inland	31.9 °/34.8 °	11.5	60	CL51 (10 m,16 s, up to 15.4 km)
Jerusalem (JR)	Mountain	31.8 °/35.2 °	53	830	CL31 (10 m,16 s, up to 7.7 km)
Nevatim (NV)	South	31.2 °/34.9 °	44	400	CL31 (10 m,16 s, up to 7.7 km)
Hazerim (HZ)	South	31.2 °/34.7 °	70	200	CL31 (10 m,16 s, up to 7.7 km)

[a]The height limit depends on sky conditions and decreases as the atmospheric optical density (AOD) increases. Data acquisition was limited to 4.5 km by the ceilometers' software (BLview), except in Beit Dagan.
[b]The location of ceilometer Beit Dagan and the radiosonde launch site.

Table 2. Parameters of the NWP models

Model	Operation center	Resolution (deg)	Type	Convection parametrization
COSMO	IMS	0.025	Regional, boundary conditions from IFS	Mass flux Tiedtke shallow convection
IFS	ECMWF	0.1 in 2015 0.125 in 2016	Global	Mass flux Tiedke-Bechtold

585 Table 3. Statistical analysis of the Beit Dagan PBL heights on 33 summer days (13 days on August 2015 and 20 days on August 2016) from IFS and COSMO models by the bulk Richardson method (IFS_R, $COSMO_R$), the parcel method (IFS_P, $COSMO_P$) and the WCT method for the adjacent ceilometer. The PBL heights were compared to those derived from Beit Dagan radiosonde by either the parcel or bulk Richardson methods (same results, see Fig 590 2).

PBL detection	IFS_R	IFS_P	$COSMO_R$	$COSMO_P$	Ceilometer
Mean Error (m)	274	271	-3	-106	12
RMSE (m)	432	411	152	176	97
R	0.18	0.21	0.83	0.83	0.93
Mean PBL (m a.s.l)	1250	1247	973	869	989
Std PBL (m)	274	245	273	222	259

Table 4. Root mean square errors of PBL heights from five sites on 13 summer days (Fig. 4), derived by IFS and COSMO models by the bulk Richardson method (IFS_R, $COSMO_R$) and the 595 parcel method (IFS_P, $COSMO_P$). The PBL heights were compared to the heights measured by the Beit Dagan ceilometer.

Site	IFS_R	IFS_P	$COSMO_R$	$COSMO_P$
Ramat David	173 m	180 m	247 m	232 m
Tel Aviv	276 m	498 m	203 m	182 m
Beit Dagan	405 m	569 m	235 m	171 m
Weizmann	214 m	339 m	175 m	209 m
Jerusalem	351 m	285 m	251 m	179 m

600 Table 5. Same as in Table 3 but for mean errors.

Site	IFS_R	IFS_P	$COSMO_R$	$COSMO_P$
Ramat David	-31 m	0 m	-26 m	-12 m
Tel Aviv	234 m	422 m	19 m	-35 m
Beit Dagan	332 m	497 m	12 m	-55 m
Weizmann	114 m	280 m	16 m	-42 m
Jerusalem	298 m	243 m	-6 m	-1 m

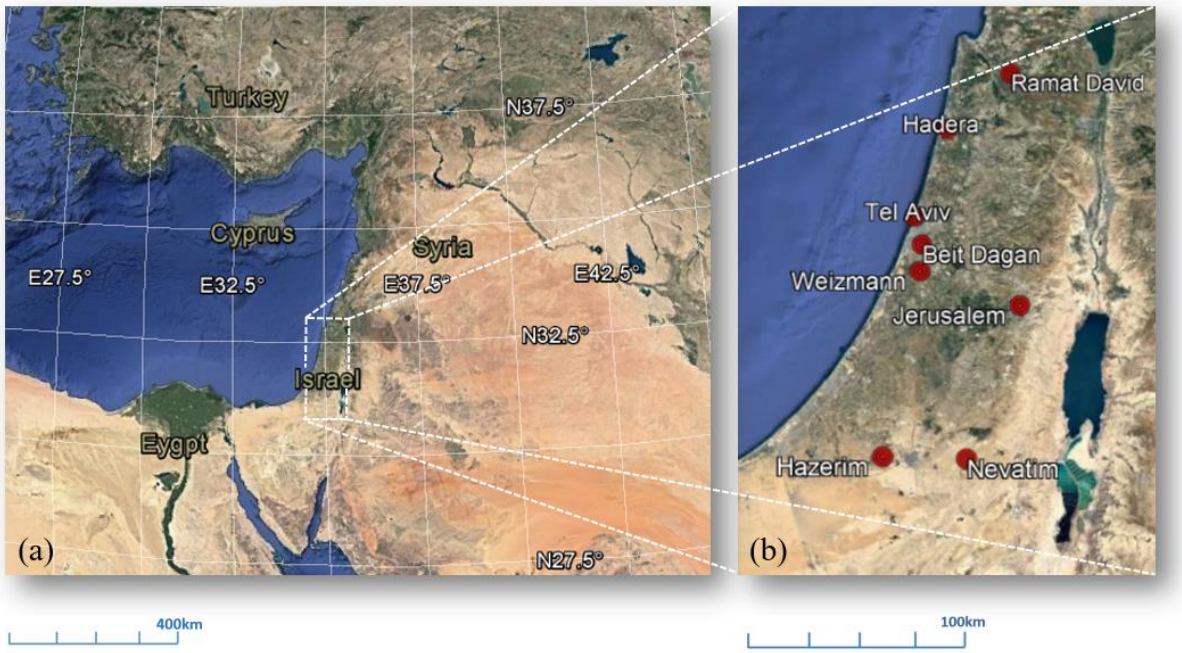

605 Fig. 1 Maps of (a) the East Mediterranean and (b) the research area including indications of the ceilometers sites (red circles). The Radiosonde launch site is situated in Beit Dagan, adjacent to the ceilometer. Adapted from © Google Maps 2019.

610

615

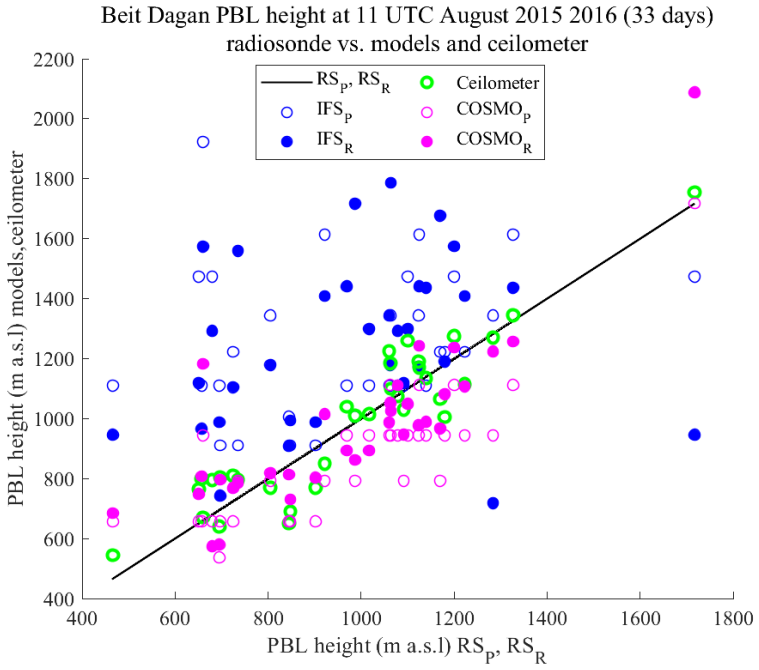

Fig 2. PBL heights over Beit Dagan site on 33 summer days (13 days on August 2015 and 20 days on August 2016), generated by the bulk Richardson method for IFS model (IFS_R, blue solid circles), COSMO model ($COSMO_R$, pink solid circles), and Beit Dagan radiosonde profiles (RS_R, black line). PBL heights generated by the parcel method for the IFS model (IFS_P, open blue circles), COSMO model ($COSMO_P$, open pink circles), and Beit Dagan radiosonde profiles (RS_P, same black line as RS_R, the results are identical). PBL heights derived from the Beit Dagan ceilometer were produced by the WCT method (green circles). Extreme Results (up to ~2, 00 m a.s.l) for August 17, 2016, are shown on the right-hand side.

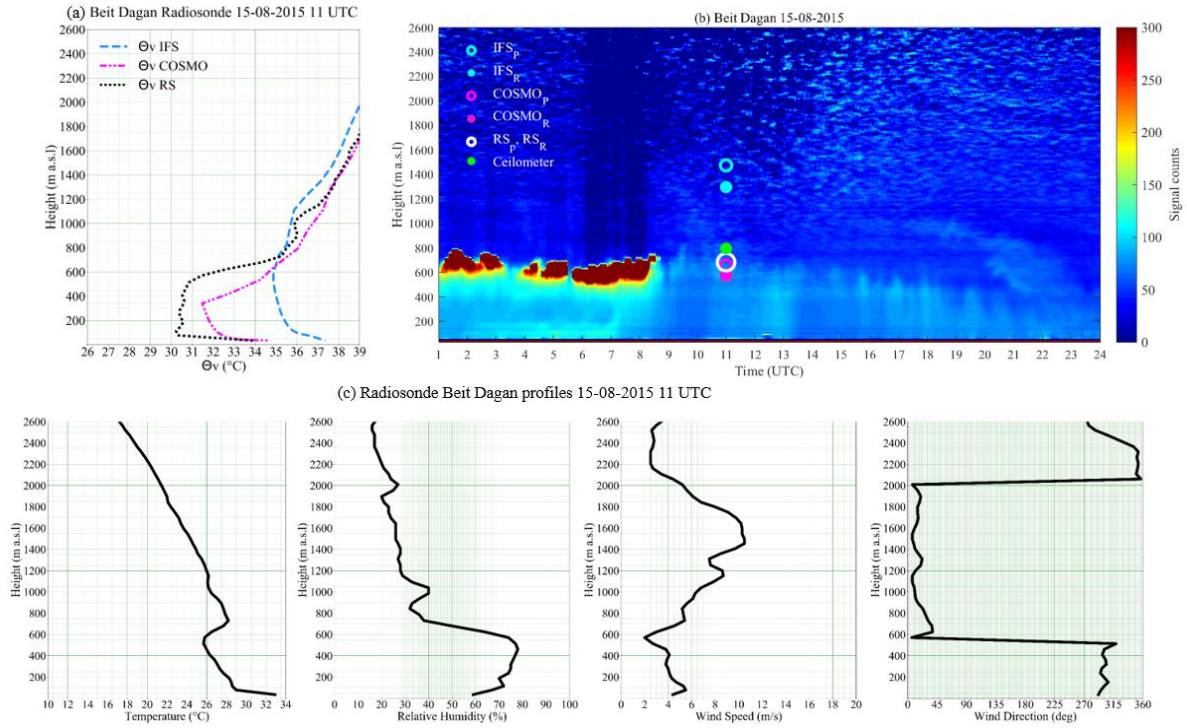

Fig.3 Meteorological measurements from Beit Dagan site on August 15, 2015: Virtual potential temperature profiles at 11 UTC generated from radiosonde measurements, IFS and COSMO models (a), ceilometer signal counts plot including indications of the PBL heights at 11 UTC from the models (IFS_R, IFS_P, $COSMO_R$, $COSMO_P$), radiosonde (RS_R, RS_P) and ceilometer (b). The bottom panel presents radiosonde profiles of temperature, RH, wind speed and wind direction at 11 UTC (c).

,

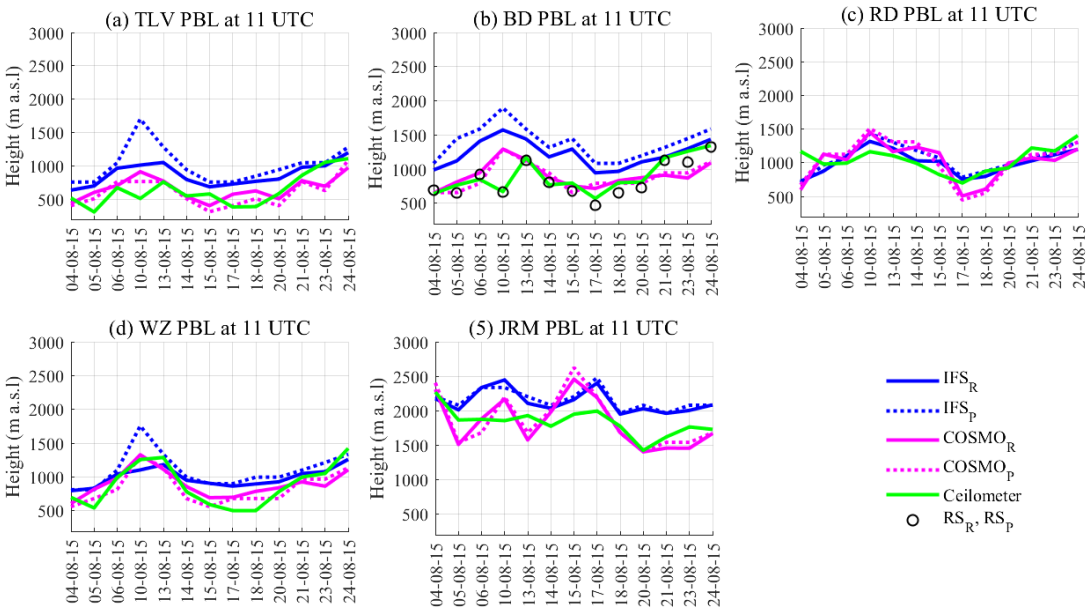

Fig. 4 PBL heights on 13 August days in 2015 from five ceilometer sites: (a) Tel Aviv (TLV), (b) Beit Dagan (BD), (c) Ramat David (RD), (d) Weizmann (WZ), and (e) Jerusalem (JRM). PBL heights were generated by the bulk Richardson method for the IFS model (IFS_R, blue solid line) and the COSMO model ($COSMO_R$, pink solid line). PBL heights generated by the parcel method for the IFS model (IFS_P, blue dashed line) and the COSMO model ($COSMO_P$, pink dashed line). Beit Dagan radiosonde profiles (RS_R, RS_P, black circles). PBL heights derived from the ceilometers (green line) were produced by the WCT method.

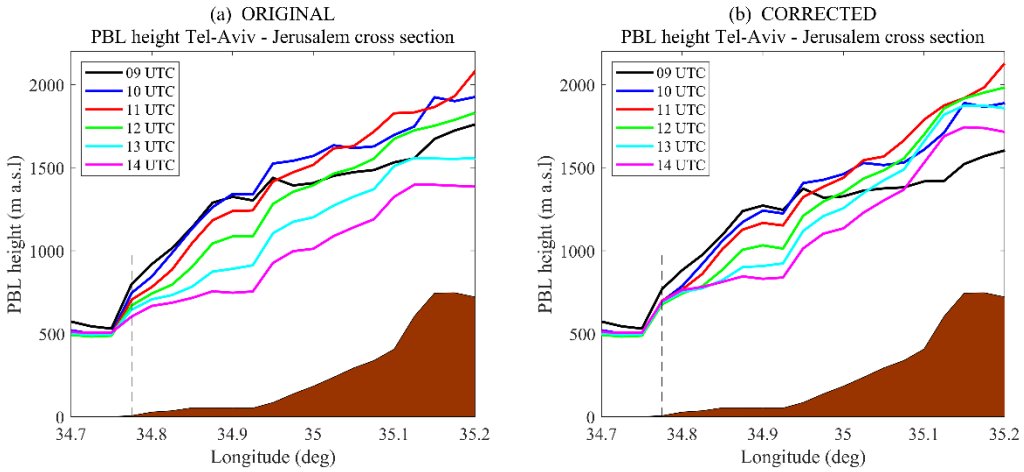

Fig. 5 $COSMO_R$ mean PBL height cross-section from Tel Aviv to Jerusalem before (a) and after (b) correction between 9-14 UTC. The analysis was performed on the number of available days for each site on August 2015 as follows: Jerusalem - 21 days, Nevatim - 13 days, Hazerim - 20 days, Ramat David - 26 days, Weizmann - 25 days, Beit Dagan - 13 days, Hadera - 16 days, Tel Aviv - 25 days. Indications of the seashore (dashed line) and the topography (brown area) are given.

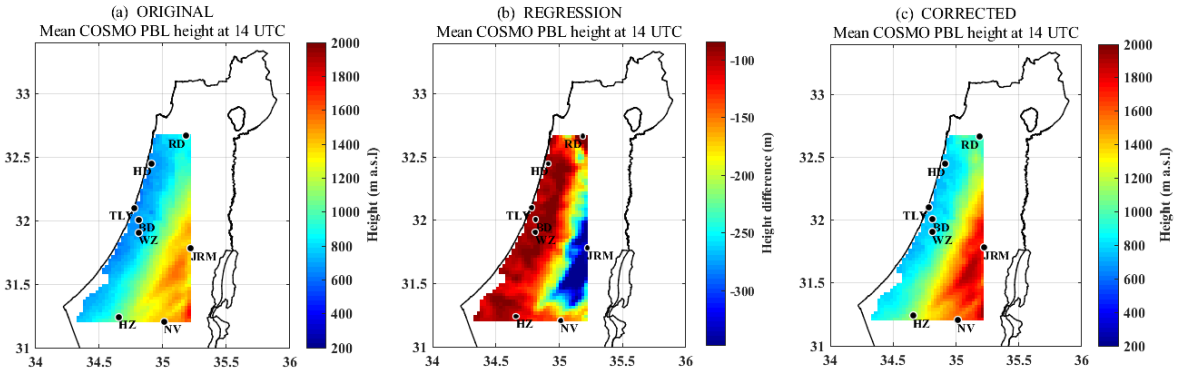

Fig. 6 3D maps of $COSMO_R$ mean PBL heights over Israel at 14 UTC before (a), and after (c) correction. The regression (b) based on Eq. (6), depicts the height difference between the results from $COSMO_R$ and the ceilometers. The analysis was performed on the number of available days for each site on August 2015 as follows: Jerusalem - 21 days, Nevatim - 13 days, Hazerim - 20 days, Ramat David - 26 days, Weizmann - 25 days, Beit Dagan - 13 days, Hadera - 16 days, Tel Aviv - 25 days.